

Alma Mater Studiorum Università di Bologna  
Archivio istituzionale della ricerca

Analysis of immiscible liquid-liquid mixing in stirred tanks by Electrical Resistance Tomography

This is the final peer-reviewed author's accepted manuscript (postprint) of the following publication:

*Published Version:*

Maluta F., Montante G., Paglianti A. (2020). Analysis of immiscible liquid-liquid mixing in stirred tanks by Electrical Resistance Tomography. CHEMICAL ENGINEERING SCIENCE, 227, 1-12 [10.1016/j.ces.2020.115898].

*Availability:*

This version is available at: <https://hdl.handle.net/11585/776754> since: 2023-02-09

*Published:*

DOI: <http://doi.org/10.1016/j.ces.2020.115898>

*Terms of use:*

Some rights reserved. The terms and conditions for the reuse of this version of the manuscript are specified in the publishing policy. For all terms of use and more information see the publisher's website.

This item was downloaded from IRIS Università di Bologna (<https://cris.unibo.it/>).  
When citing, please refer to the published version.

(Article begins on next page)

# **Analysis of immiscible liquid-liquid mixing in stirred tanks by Electrical Resistance Tomography**

Francesco Maluta<sup>a</sup>, Giuseppina Montante<sup>a</sup>, Alessandro Paglianti<sup>b</sup>

<sup>a</sup>Department of Industrial Chemistry, Università di Bologna, via Terracini 28, 40131 Bologna, Italy.

<sup>b</sup>Department of Civil, Chemical, Environmental and Materials Engineering, Università di Bologna, via Terracini 28, 40131 Bologna, Italy.

## **Abstract**

In this work, the dispersion of diesel fuel in water in a baffled tank stirred by a Rushton turbine is investigated. The impeller speeds corresponding to the initial drawdown, the just dispersed regime and the completely dispersed regime are identified by suitable variables obtained by means of the Electrical Resistance Tomography technique. The effect of the dispersed phase volume fraction and of the impeller off-bottom clearance on the different dispersion regimes is considered. The impeller Froude number, the Archimedes number and a dimensionless distance between the liquid-liquid interface position and the impeller elevation are adopted for the data interpretation. For the investigated system, the local volume fraction profiles show that the completely dispersed condition is practically achieved above the just dispersed impeller speed, with negligible gradients of the local volume fraction distribution in the axial direction.

**Key words:** Mixing; liquid-liquid regimes; Electrical Resistance Tomography, initial drawdown, completely dispersed.

## 1. Introduction

Immiscible liquid-liquid dispersions are relevant in several industrial applications of chemical, pharmaceutical, food, polymerisation and petroleum sectors, among others for example, as reported by Du et al. (2019), for the separation of light oil pyrolysis and platinum reforming, multiphase catalytic processes for pharmaceuticals and fine chemicals, reuse of soluble polymer-supported catalysts, extraction of rare-earth elements, nitrification, sulfonation.

Depending on the different drop sizing objectives, on the power requirements and on the process conduction (batch or continuous), different equipment options are available from an industrial perspective, such as baffled and unbaffled stirred tanks, static mixers, rotor-stator mixers, impingement mixers, and ultrasonic mixers among the others. Stirred tanks are often selected for the mixing operation, with the aim of obtaining a dispersion of droplets with size distribution in the continuous liquid ranging from around 30  $\mu\text{m}$  to few millimeters (Leng and Calabrese, 2016). In operations where local high-shear is desired, fully baffles stirred tanks and radial turbines are commonly adopted, with the most common impeller being the Rushton turbine (Hemrajani and Tatterson, 2004).

Obtaining a dispersion of droplets with specific size distribution is a very challenging task, due to the complex nature of turbulent two-phase flows that is further complicated by the shape deformation of the droplets, with respect to the case of solid particle dispersions (Elghobashi, 2019). Occurrence and interaction of several aspects, such as turbulence, drop break-up and coalescence, drop suspension, interfacial area, possible phase inversion, influence of the liquids composition and physical properties, make this operation one of the most difficult to deal with in stirred tanks (Afshar Ghotli et al., 2013; Leng and Calabrese, 2016).

In order to control the features of the dispersion and to optimize the energy consumption simultaneously, the agitation conditions and the geometry of the stirred tank must be selected with care. Significant efforts on both the experimental and the computational sides have been devoted so far to the understanding of the fundamentals of the fluid dynamics interaction between the two phases and to the development of predictive methods for improving the equipment performances and the quality of the products. Breakup and coalescence phenomena, mean and minimum drop size have been studied from an equipment scale (Calabrese et al., 1986; Maaß et al., 2007; Zhou and Kresta, 1998), to a scale comparable with the impeller dimensions (Liang et al., 2019; Maaß et al., 2009; Solsvik and Jakobsen, 2015) and further down to the droplet scale (Kamp and Kraume, 2016; Komrakova et al., 2015; Maaß et al., 2012) with the aid of numerical simulations, focusing on the relevant fluid dynamics scales and interactions.

From an equipment point of view, some empirical correlations to estimate the agitation speed necessary to achieve the complete liquid-liquid dispersion are already available (Nagata, 1975; Skelland and Ramsay, 1987; Skelland and Seksaria, 1978). Most of the experimental data were collected by sampling techniques (Armenante and Huang, 1992; Kamil et al., 2001; Mehta, 2002).

Notwithstanding the tremendous improvements gained in the recent past, average properties over the whole vessel are usually considered for system description and for scale-up, particularly in the case of concentrated liquid-liquid systems. Some of the more detailed studies focus on the scale-up effects on the drop size when the secondary phase is completely dispersed in the continuous phase (Bałdyga et al., 2001; Podgórska, 2005; Podgórska and Bałdyga, 2001) or the effect of surfactants (Mirshekari, et al., 2019).

Modelling methods have also been developed by fully-predictive, two-phase Computational Fluid Dynamics (CFD) techniques coupled with break-up and coalescence models (Alopaeus et al., 2002; Derksen and Van Den Akker, 2007; Li et al., 2017; Maaß et al., 2010, 2007; Vonka and Soos, 2015), but their adoption to full scale equipment is still a challenge.

One key issue for moving towards cases of industrial interest and allowing CFD code validation under conditions close to industrial applications is to obtain quantitative data in concentrated liquid-liquid systems. To this end, the application of Electrical Resistance Tomography (ERT) appears particularly appropriate, as shown among the first by Ricard et al. (2005), whose focus was on the monitoring of pharmaceutical processes. A meaningful picture of the wide range of applications of ERT to the investigation of industrially relevant mixing operations has been recently provided by Bowler et al. (2020). As also reported by Naeeni and Pakzad (2019), ERT has been used for the investigation of many single-phase and two-phase systems in stirred vessels, but very few studies so far concerned liquid-liquid systems. The effectiveness in evaluating the liquid-liquid mixing performances based on ERT data was shown by Mirshekari and Pakzad (2019), who compared the effect of different physical properties of the liquid-liquid dispersions and different geometrical characteristics of the stirred vessels based on a mixing index obtained on two measuring planes. Additional investigations in the field of immiscible liquid-liquid mixing based on ERT can be very useful, considering the important achievements already obtained for instance in the study of the non-Newtonian liquid mixing (Kazemzadeh et al., 2016), the solid suspension (Harrison et al., 2020) and the gas dispersion (Forte et al., 2019) in stirred tanks.

Among the different aspects that have been studied so far, the agitation speed to obtain different liquid-liquid dispersion regimes and the relevant volume fraction distribution of the dispersed

phase in the continuous liquid are specifically addressed in this work, with special focus on the methodology to collect reliable data and to evaluate the transitions between the different regimes. The investigated diesel fuel-water mixture has similar physical properties of other liquid-liquid systems used for the analysis of bioreactors for biodesulfuration of crude oil (Tsouris et al., 1996), for the analysis of drops coalescence and breakage in stirred tanks (Daglas & Stamatoudis, 2000, De Bona et al., 2016), for the analysis of macromixing phenomena (Zhao et al., 2011), for the analysis of homogeneously catalysed hydroformylation of olefins (Hohl et al., 2019), for the isobutene alkylation (Duan et al., 2019).

The paper is organized as follows: in the next section, the experimental system and the technique adopted for collecting the experimental data are presented. Afterwards, the dimensionless conductivity maps obtained in typical experimental runs and the main features and limitations of the data under various experimental conditions are addressed. Then the liquid-liquid regimes, the definition of the variables for identifying the transition between them are provided together with dimensionless numbers to identify the relevant liquid-liquid dispersion regimes with respect to specific combination of parameters (impeller speed, dispersed phase volume fraction, impeller clearance). Finally, a close look to the spatial distribution of the droplet volume fraction under selected conditions is presented.

## **2. Material and methods**

### *2.1 The stirred tank configurations and the liquid-liquid system*

The investigation was carried out in a cylindrical, flat bottomed stirred vessel made of Plexiglas of diameter,  $T$ , equal to 0.232 m and height,  $H$ , equal to 0.28 m. Four equally spaced baffles of width,  $W$ , equal to  $T/10$  were fitted to the vessel wall to prevent the central vortex formation and

to enhance the action of the impeller. Agitation was provided by a single Rushton turbine of diameter,  $D$ , equal to  $T/3$ , mounted on a central shaft, located alternatively at the off-bottom clearance,  $C$ , of  $T/3$  or  $T/2$ . The main geometrical features of the stirred vessel are shown in Figure 1, where the location of the electrodes for the ERT measurements is also specified.

The liquid-liquid system consisted in demineralised water and commercial diesel fuel. The physical properties of the two liquids are summarized in Table 1.

Table 1. Physical properties of the two liquids at 25°C.

	<i>Density, <math>\rho</math> [kg/m<sup>3</sup>]</i>	<i>Viscosity, <math>\mu</math> [Pa s]</i>	<i>Surface tension, <math>\sigma</math> [mN/m]</i>
<b>Water</b>	997	$8.90 \times 10^{-4}$	72.0
<b>Diesel fuel</b>	826	$3.50 \times 10^{-3}$	27.6

A necessary prerequisite for the ERT application to two-phase flows is to have an appropriate conductivity difference between the two phases (Stanley, 2006). For this reason, 5 g/L of NaCl were added to the conductive phase, that is the demineralized water in this case, while the diesel fuel conductivity was assumed to be nil. The small amount of salt was assumed to be uninfluent on the demineralized water physical properties.

The investigated experimental conditions are summarized in Table 2.

Table 2. Summary of the investigated experimental conditions.

	Oil volume fraction, $\phi_d$ [-]	Impeller speed, N [rpm]	Impeller Reynolds number, Re [-]
Investigated range	0.05-0.5	100-600	$1.1 \times 10^4$ - $7.0 \times 10^4$

The diesel fuel volume fraction in the tank was varied from dilute to concentrated conditions. Starting from the fluid at rest, the impeller speed,  $N$ , was increased stepwise from 100 rpm up to 600 rpm. Based on the impeller Reynolds number,  $Re$ , that was calculated with the water physical properties, the flow regime was fully turbulent. The total liquid height,  $H_L$ , was maintained at 0.232 m, corresponding to a total volume of 9.81 L. The experiments were carried out at the room temperature of 25°C in batch conditions.

## *2.2 The Electrical Resistance Tomography technique*

The local distribution of the diesel fuel in water was evaluated on four horizontal sections of the vessel from the local conductivity of the liquid-liquid mixture measured with the ITS 2000 ERT instrumentation (Industrial Tomography Systems Ltd). The measurement set-up is schematically depicted in Figure 1. The vessel periphery was provided with equally spaced electrodes, made of squared stainless steel plates (20x20 mm, 1mm thickness). The electrodes were fixed to the internal vessel wall at four horizontal elevations, located at  $z_1=60\text{mm}$ ,  $z_2=110\text{mm}$ ,  $z_3=160\text{mm}$ ,  $z_4=210\text{mm}$  from the vessel bottom. For each plane, 16 electrodes were adopted. As a result, the impeller was located between the planes  $z_1$  and  $z_2$  for  $C=T/3$  and between  $z_2$  and  $z_3$  for  $C=T/2$ . The electrodes were then connected to the Data Acquisition System (DAS) by coaxial cables. The measurements were based on the so-called circular adjacent strategy, in which electric current is injected from adjacent electrodes pair at a time and the voltage difference is measured from the remaining pairs of electrodes. The procedure is repeated for all the independent pairs of electrodes.



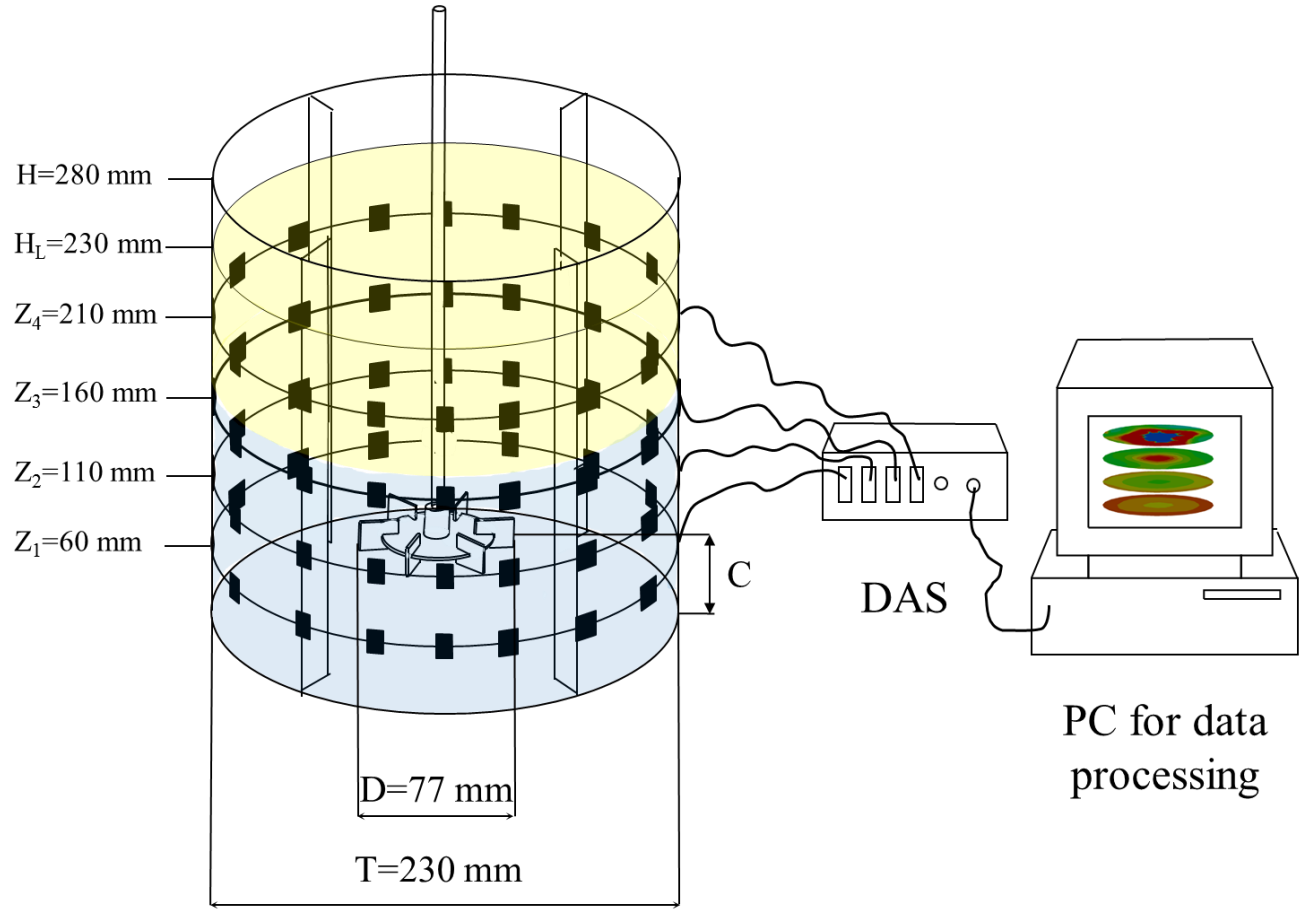


Figure 1. Schematic characteristics of the experimental system.

As for the reconstruction method for obtaining the conductivity maps from the electric potential measurements, the linearized (non-iterative) modified sensitivity back projection (MSBP) algorithm was selected (Wang et al., 1996), as implemented in the ITS System p2+ V8 software. The reconstruction of the conductivity maps was very fast, thus the phase distribution was monitored in real time.

The local conductivity on each plane was obtained on a mesh of 11.6 mm x 11.6 mm. The number of local measurements inside each circular tomogram,  $n$ , was equal to 316, thus, when considering the 4 investigated planes, a total number of conductivity values,  $p$ , equal to 1264 was obtained. The amplitude and the frequency of the injected current were set at 15 mA and 9600

Hz respectively, after preliminary calibration tests. For each set of acquisitions, 600 total instantaneous measurements were collected, at a frequency of 0.92 frames per second.

In the following, the results of the measurements are shown in terms of dimensionless local conductivity,  $X_i$ , that is computed as the ratio between the local conductivity,  $\gamma_i$ , measured in the liquid-liquid mixture and a reference conductivity  $\gamma_i^{ref}$ . . The data analysis is based on the ensemble average of the instantaneous dimensionless conductivity. The estimated error on the local conductivity, based on triplicate measurements, is equal to 3%.

### *2.3 Reference measurements and fringe effect*

In the case investigated in this work, the dimensionless conductivity can be either measured with respect to the unstirred segregated two-phase system with the lighter phase floating on top of the heavier phase or in the unstirred single-phase system containing only the continuous conductive phase filling the vessel up to  $H_L$ . To the best of our knowledge, all the previous investigations based on ERT measurements in liquid-liquid systems did not tackled the issues described in the following, either due to the limited volume fraction of the non-conductive phase (Naeeni and Pakzad, 2019) or to the position of the electrodes far enough from the non-conductive liquid level (Mirshekari and Pakzad, 2019). Instead, for the conditions investigated in this work, depending on the choice of the reference measurement, significantly different results are obtained, as can be observed in Figure 2, where, by means of example, the radial profiles of the dimensionless conductivity,  $X$ , obtained with different references are reported. The radial profiles are obtained from the tangential average of the measured  $X_i$  on  $z_3$ . Figure 2(a) refers to measurements at a low impeller speed, when the two phases are completely segregated, with the interface located at  $z_I=221$  mm. Although, at the selected agitation condition, from visual

observations the diesel fuel is completely segregated on top of the water, the profile obtained with the reference taken with the aqueous water solution only shows a considerable decrease of dimensionless conductivity, especially towards the centre of the vessel, while a constant profile is obtained using the measurements in the still oil-water system as the reference.

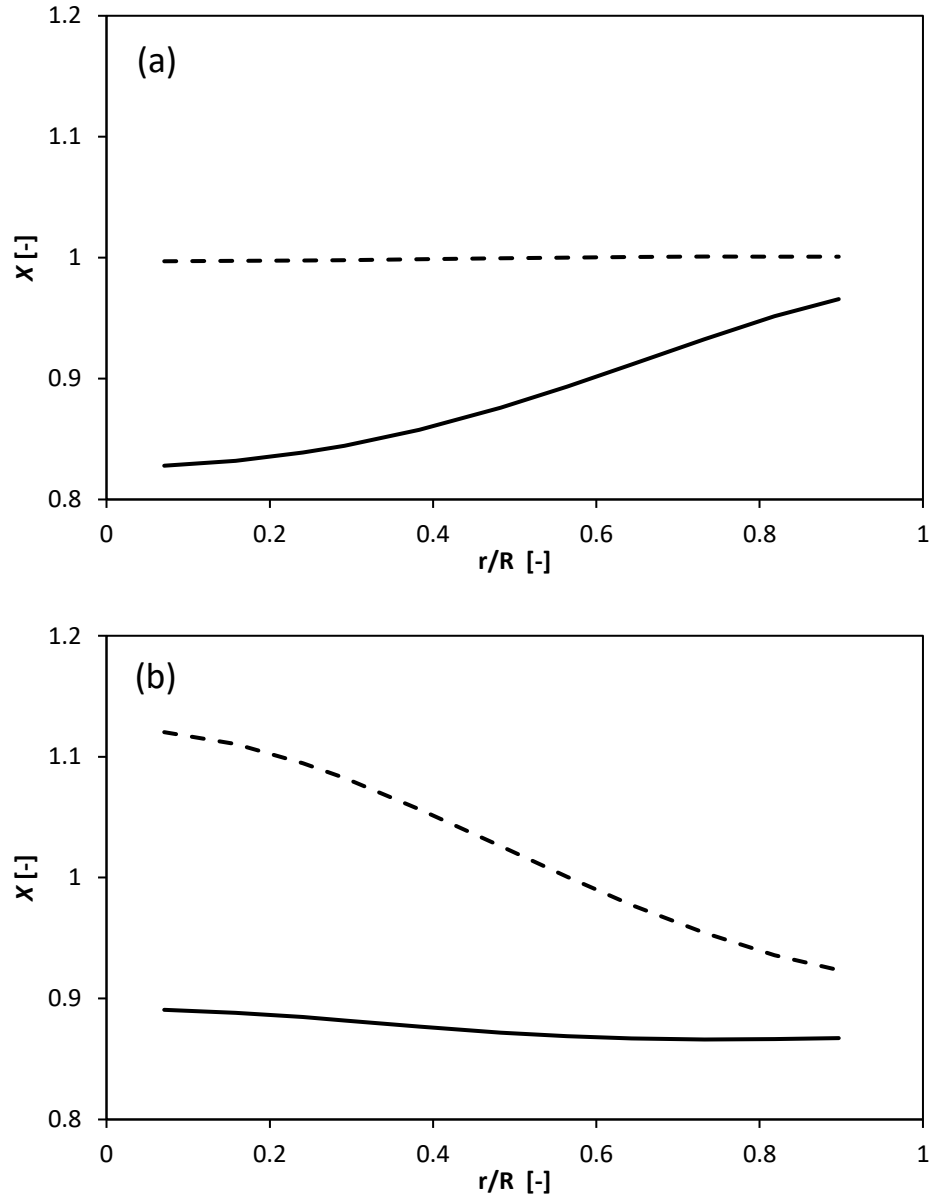


Figure 2. Radial profiles of dimensionless conductivity on  $z_3$  obtained with reference measurements in still water (solid line) and still oil/water mixture (dotted line),  $\phi_d = 0.05$ ,  $C=T/3$ .

(a)  $N=170$  rpm (stratified condition); (b)  $N=520$  rpm (completely dispersed condition).

This observation could lead to the conclusion that the reference measure has to be taken with the oil-water system at rest, since it provides reliable results. On the other hand, Figure 2(b) shows the experimental data at impeller speeds high enough to have complete dispersion of the lighter phase in the heaviest. In this case, the exact opposite result is obtained, in fact, in these conditions the dimensionless conductivity becomes larger than unity towards the centre of the vessel for the reference measurements taken with water and diesel fuel at rest.

This behaviour is most likely due to the fringe effect (Lioumbas et al., 2014; Sun and Yang, 2013) that extends the measuring field outside the electrodes plane, as shown in Figure 3. This effect is known in the community of the sensor developers, but it has been rarely taken into account in the fluid dynamic analysis of the equipment.

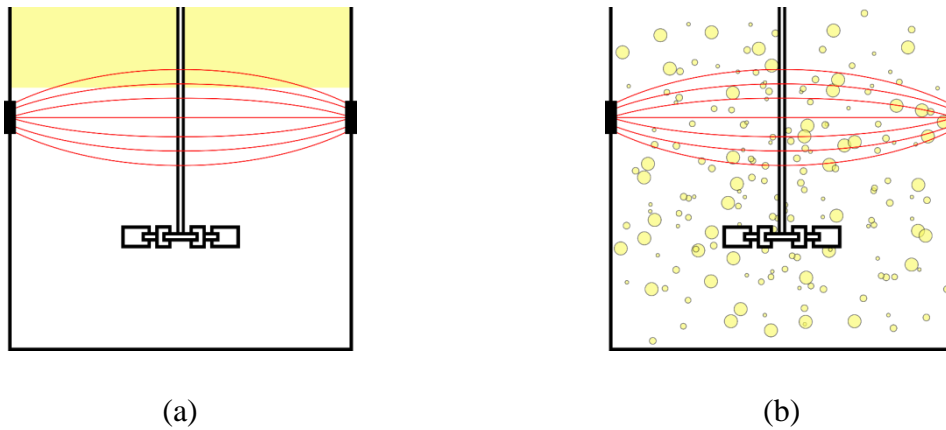


Figure 3. Scheme of the electric field (red lines) generated by an electrode plane in the two phase system. (a) phase distribution at low impeller speed; (b) phase distribution at high impeller speed.

In segregated liquid-liquid systems, the sensors on the plane close to the oil/water interface register the presence of the non-conductive phase even though the liquid-liquid interface is above

the measuring plane, as can be observed in Figure 3(a). When this measurement is compared with the reference taken with just the conductive phase, the resulting dimensionless conductivity indicates that non-conductive phase is present on the measurement plane, that is not real. The measured conductivity becomes smaller toward the centre of the vessel, where the fringe effect is larger, as shown by the solid line in Figure 2(a). On the other hand, comparing the measurement with the reference taken with the water-diesel fuel mixture results in a constant radial profile of dimensionless conductivity equal to 1, in agreement with the visual observations (dotted line, Figure 2(a)).

For completely dispersed conditions, that are depicted in Figure 3(b), if the reference is obtained from a stratified oil/water mixture, the local conductivity in the centre of the tank is greater than that measured in the reference condition. Therefore, the dimensionless conductivity assumes values greater than one, that is clearly wrong, as shown by the dotted line in Figure 2(b). Conversely, if the reference is measured with the conductive phase only, the ratio between the conductivity of the oil/water mixture and the water phase provides physically consistent results (solid line, Figure 2(b)). Indeed, the measurements at high impeller rotational speeds obtained with the single-phase reference produce an almost constant radial profile in agreement with the homogeneous dispersion conditions expected at high impeller rotational speeds. From these observations, it follows that the choice of the reference affects the results and, one way or another, produces uncertainties.

As an additional example of the issue described above, the case of a high oil volume fraction of oil is shown in Figure 4, where the dimensionless conductivity on the four measurement planes,  $X_i$ , is obtained adopting the single-phase reference conductivity. The vertical values are obtained from a numerical interpolation of the measurements on the four measuring planes.

Being the electrical conductivity of the oil negligible with respect to that of the water, the dimensionless conductivity is bounded between 1 (water only) and 0 (oil only). In this case the oil/water interface in still conditions,  $z_I$ , is located at 151 mm, that is below both the  $z_3$  and the  $z_4$  planes. As a result, the measurements at slower impeller speed shown in Figure 4(a) are not reliable in the upper two planes, since at  $N=220$  rpm the electrodes are still fully immersed in a non-conductive phase. Increasing the impeller speeds of a few tens of rpm the partial drawdown of the oil takes place, but the measurements on  $z_4$  do not provide reliable data because of the presence of a thick oil layer, as shown in Figure 4(b). Instead, the measurements are reliable on the whole set of elevations when the oil is completely dispersed, as in the case of the results shown in Figure 4(c).

Overall, using the single-phase reference, the ERT conductivity maps show a physically consistent representation of the liquid-liquid system, provided that the electrodes are not immersed and are far enough the non-conductive phase continuous layer.

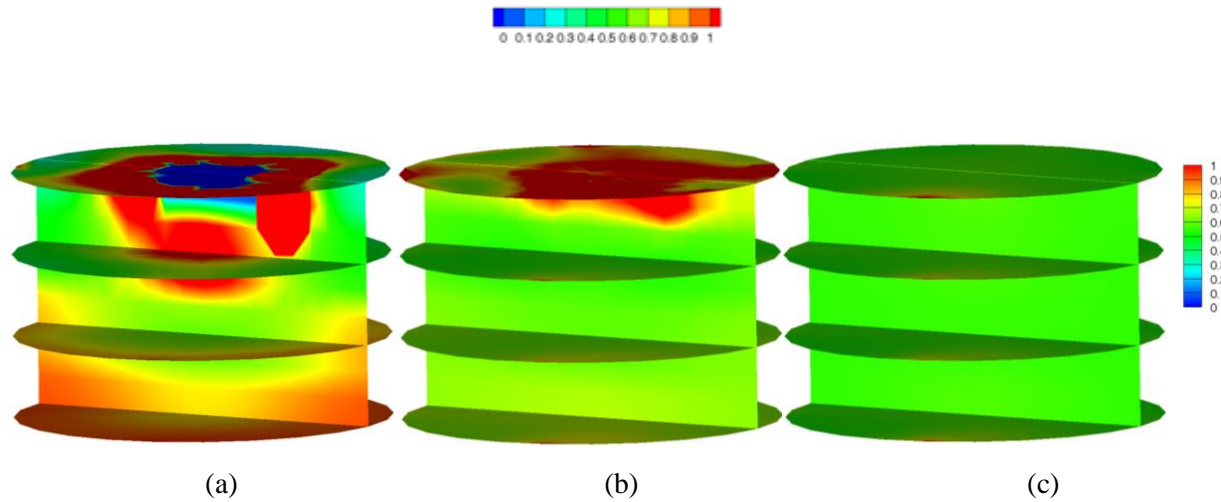


Figure 4. 3D-map of dimensionless conductivity  $X_i$ ,  $C/T=1/2$ ,  $\phi_d=35\%$ . (a)  $N=220$ rpm; (b)  $N=250$  rpm; (c)  $N=460$  rpm.

Keeping in mind these limitations of the technique, the data have been collected with the reference measurement in the vessel filled with just water at rest. The data collected at low impeller rotational speeds have been specifically treated depending on the purpose of the analysis, as discussed in the following.

### **3. Results and Discussion**

#### *3.1 Definitions and methodology for the identification of dispersion regimes*

A method for estimating the characteristic regimes of liquid-liquid mixing and the transitions from one regime to another can be defined with ERT data and through the definition of suitable variables accounting for the distribution of the two liquids in the vessel volume as a function of the geometrical and operating variables. In the literature, two regimes are most frequently considered, the “just dispersed” (JD) condition, where no continuous layer of the dispersed phase is present in the vessel, and the “completely dispersed” (CD) conditions, where the mixture is uniformly distributed in the tank. An additional condition can also be considered, that is the “initial drawdown” (ID), corresponding to the beginning of droplets entrainment in the heavier liquid phase (Brown et al., 2004).

In the following, the different regimes as depicted in Figure 5 will be considered.

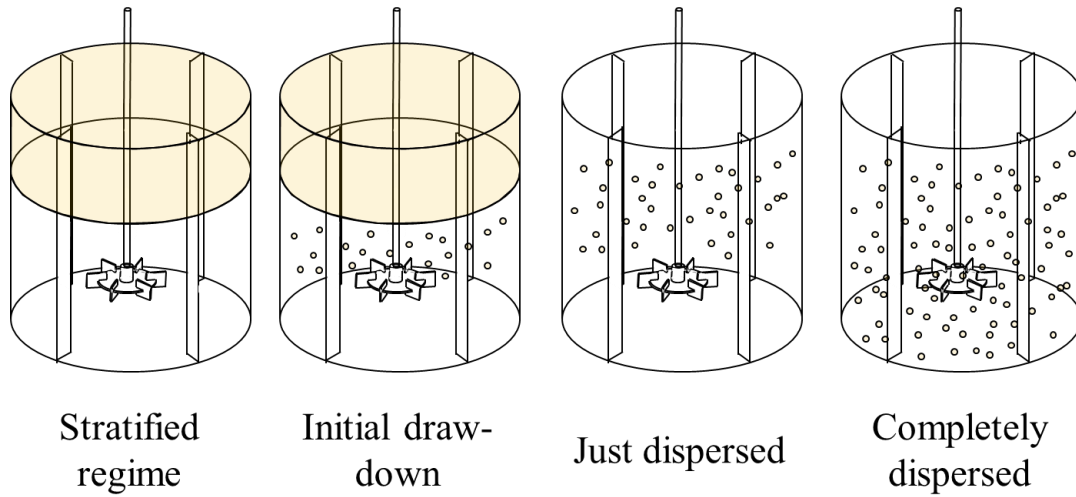


Figure 5. The characteristic regimes of immiscible liquid-liquid mixing.

The transitions from one regime to another have been identified from the conductivity measurements on the four planes.

*Stratified/initial drawdown*: the transition between the stratified and the initial drawdown occurs at the impeller speed at which droplets of diesel fuel detach from the coherent layer on the top of the vessel and they are entrained in the bulk of the heavier phase. For this reason, the determination of the impeller speed at the initial drawdown was performed on a single measurement plane, that was selected depending on  $\phi_d$ . In particular, the highest plane below the elevation of the liquid-liquid interface at rest,  $z_l$ , was considered. Obviously, the drawdown phenomenon has to be analysed starting from a free oil layer on the top of the tank. In these conditions, the results reported in Figure 2(a) suggest to use the still oil/water mixture as the reference, that, on the other hands, leads to large errors when the mixture in the tank approaches the dispersion conditions, as shown by the results in Figure 2(b). To overcome this issue, the difference between the dimensionless conductivity obtained at the impeller speed,  $N$ , using as reference the still oil/water mixture and the dimensionless conductivity obtained at still



conditions (N=0 rpm) with the same reference should be considered. This difference can be expressed as:

$$\Delta X(N) = \left| \frac{\gamma_{i,N}}{\gamma_{i,N=0}^{ref,oil/water}} - 1 \right| \quad (1)$$

that can be simply re-arranged as:

$$\Delta X(N) = \left| \frac{\frac{\gamma_{i,N}}{\gamma_{i,N=0}^{ref,water}} - \frac{\gamma_{i,N=0}}{\gamma_{i,N=0}^{ref,water}}}{\frac{\gamma_{i,N=0}}{\gamma_{i,N=0}^{ref,water}}} \right| \quad (2)$$

In this form the equation evidences that to identify the initial drawdown the reference can be recorded with the water phase, avoiding the need to adopt different reference measurements depending on the liquid-liquid regime.

Finally, in order to evaluate the initial drawdown impeller speed, the maximum relative deviation from the initial condition of oil-water system at rest is evaluated, as:

$$\Delta X_{max}(N) = \max \left| \frac{X_{i,N} - X_{i,N=0}}{X_{i,N=0}} \right| \quad (3)$$

where the dimensionless conductivities are obtained using the reference with the water phase only. The variation of  $\Delta X_{max}$  as a function of N is shown for the specific system in Figure 6. As can be observed, at the lower values of the investigated agitation speeds, when the regime is stratified, the calculated maximum difference defined by Eq. (3) is almost constant, but not nil, due to the interface movement, that leads to conductivity maps slightly different from that measured in still conditions. The abrupt increase observed between N=200 rpm and N=250 rpm correctly catches the initial significant drawdown, confirmed by the visual observation of the tank, because the ERT data detect the entrainment of oil droplets in the water phases by the conductivity variation with respect to the stratified regime.

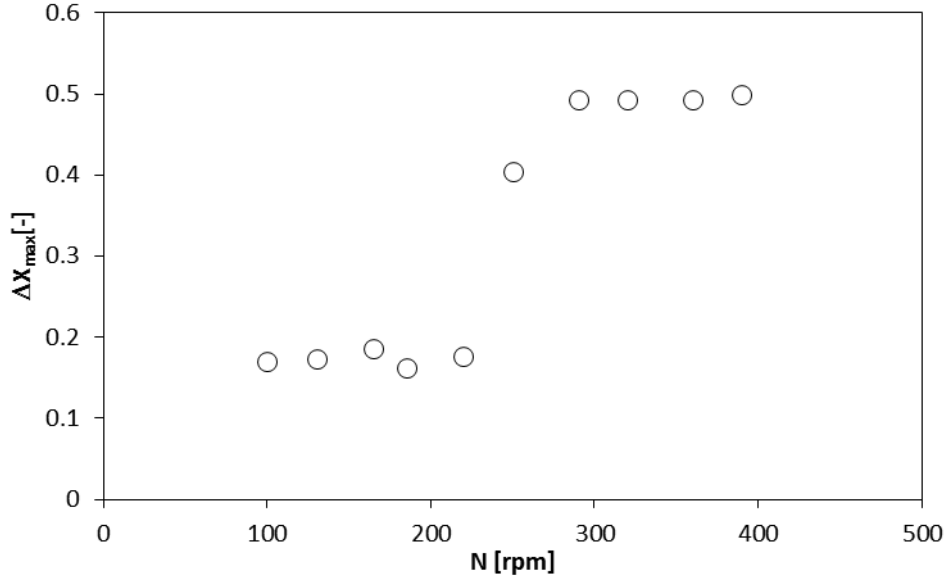


Figure 6. Maximum local dimensionless conductivity difference vs impeller speed on  $z_2$  (highest plane below the  $z_I$  elevation).  $C/T=1/2$ ,  $\phi_d=35\%$ .

It is worth noticing that the advantage of ERT over local probes is to provide local information on a whole section. On the other hand, it is important to point out that the ERT is insensitive to the decrease in conductivity due to very few droplets. Moreover, the drawdown is visually identified as the droplets are entrained from the coherent liquid layer into the continuous phase, in the close proximity of the liquid-liquid interface, whereas the ERT registers the drawdown as the nonconductive droplets reach the measurement plane, that is located at some distance from the liquid-liquid interface. For these reasons, the stratified/initial drawdown transition is identified by the ERT at higher impeller speed with respect to the visual observation based on the first entrained droplet. Keeping in mind that the dimensionless conductivity in each cell of the plane is the average of multiple frames, it is reasonable to think at the maximum deviation as a probability to find oil droplets in one of the measurement plane locations and said probability increases as the impeller speed increases.

*initial drawdown/just dispersed*: by definition, the transition between the two regimes takes place when the continuous layer of the dispersed phase disappears from the vessel top region (or from the bottom, in case of a dispersed phase denser than the continuous liquid). To identify this transition the conductivity on the  $z_4$  plane is considered, being this plane closer to the coherent oil layer elevation when most of the drawdown is accomplished. At very high volume fractions of the diesel fuel, it becomes the continuous phase, therefore the plane  $z_1$  is considered, as it is the closer to the coherent water layer located on the vessel bottom. For detecting the transition between the two regimes, the mixing index on the plane,  $MI_z$ , as adopted by (Carletti et al., 2014), was calculated as:

$$MI_z = \frac{1}{\bar{X}} \sqrt{\frac{\sum_{i=1}^n (X_i - \bar{X})^2}{n-1}} \quad (4)$$

Where  $\bar{X}$ , is the mean dimensionless conductivity value on  $z_4$ ,  $X_i$  is the local dimensionless conductivity and  $n$  is the number of measurements on the plane.

In Figure 7 values of  $MI_z$ , obtained for the same condition analysed in Figure 6, are shown. The transition can be identified at the impeller speed of 300 rpm, at which  $MI_z$  reaches a very low value, corresponding to the homogeneity on the plane, as confirmed by the visual observation of the tank. It is interesting to notice that, adding to the analysis the mixing index definition of Harrison et al. (2012), the same critical velocity is obtained.

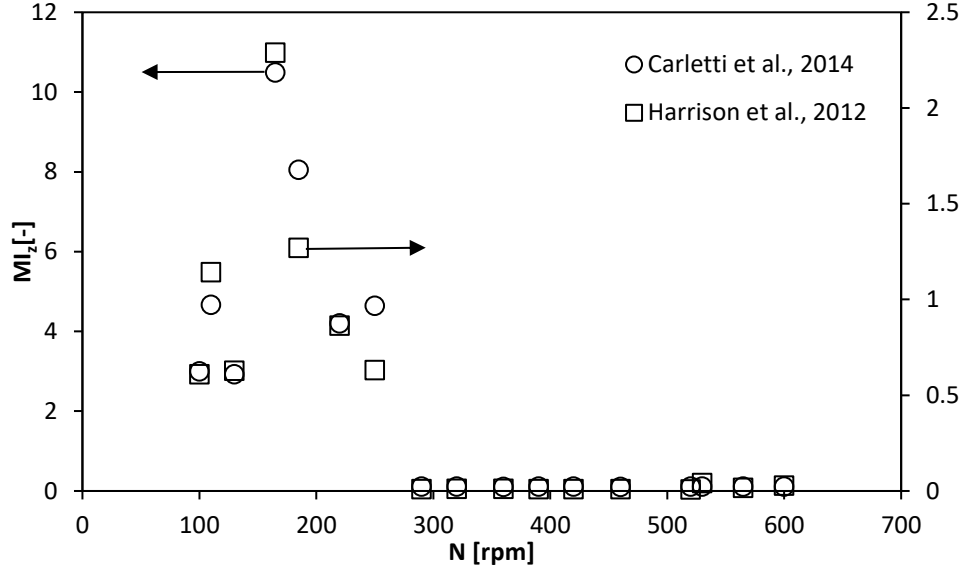


Figure 7. Mixing index on the highest measurement plane vs impeller speed.  $C/T=1/2$ ,  $\phi_d=35\%$ .

*just dispersed/completely dispersed*: this transition occurs when the liquid–liquid dispersion is distributed uniformly throughout the vessel. Differently from the previous transitions, it cannot be estimated by the visual observation of the tank and it is generally difficult to detect (Brown et al., 2004). The following definition of the overall mixing index from ERT data is adopted, as proposed for the analysis of solid-liquid systems by Carletti et al. (2014):

$$MI_{tot} = \frac{1}{\bar{X}} \sqrt{\frac{\sum_{i=1}^p (X_i - \bar{X})^2}{p-1}} \quad (5)$$

where  $p$  is the total number of measurements in the four measurement sections and  $\bar{X}$ , is the mean dimensionless conductivity on the four sections.

The  $MI_{tot}$  calculated at the different impeller speeds, shown in Figure 8, clearly identifies the condition of complete dispersion corresponding to the sudden drop to a constant lower value, that for the selected condition occurs at 300rpm. This result, as in the case shown in Figure 7,

does not depend on the MI definition used for the evaluation. Comparing the dependency of  $MI_{tot}$  on  $N$  shown in Figure 8 with that of  $MI_z$  shown in Figure 7, it is apparent that the same agitation condition that ensures the just dispersed regime allows to uniformly disperse the oil droplet in the tank, for the specific system under consideration. This finding is most likely associated with the relatively small density difference between the two liquids and the geometrical characteristics of the tested stirred tank.

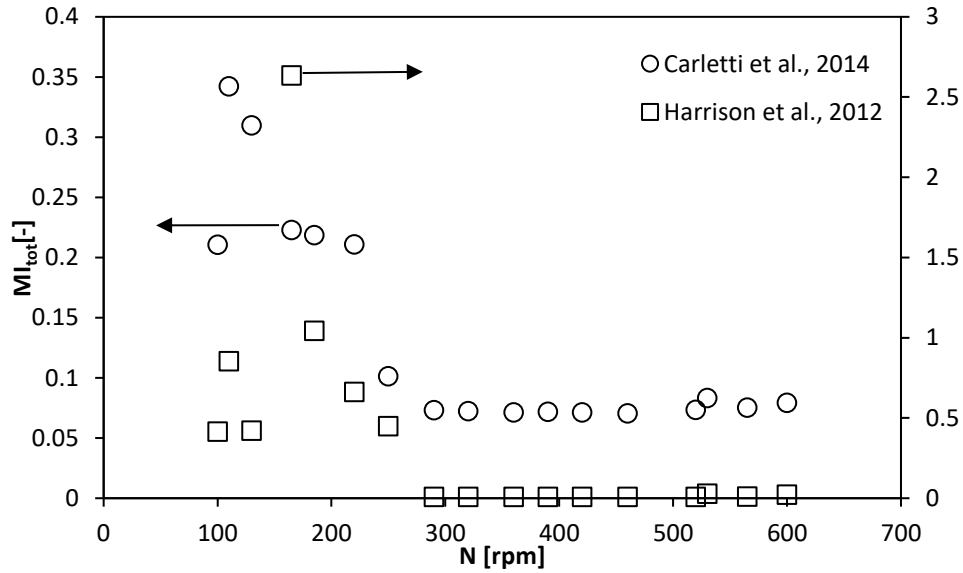


Figure 8. Total mixing index vs impeller speed.  $C/T=1/2$ ,  $\phi_d=35\%$ .

### 3.2 Dimensionless parameters for the identification of a liquid-liquid dispersion map

#### 3.2.1 Initial drawdown impeller speed, $N_{ID}$

The variables defined in the previous sections and the methods for identifying the regime transitions have been considered for the whole set of the experimental conditions, in order to build a map for the identification of the liquid-liquid dispersion regimes in baffled tanks stirred by Rushton turbines. Clearly more geometrical variations, different dimensions of the stirred

tanks and a much wider range of physical properties of the two liquids will be required to achieve conclusive results.

In Figure 9, the initial drawdown impeller speed,  $N_{ID}$ , is shown as a function of the oil volume fraction for the two impeller clearances of  $T/2$  and  $T/3$ . A clear reduction of  $N_{ID}$  at increasing  $\phi_d$  is detected, and a limited effect of the clearance is observed at equal  $\phi_d$ . As expected, the results show that higher agitation speed is required for achieving the initial drawdown as the distance of the liquid-liquid interface from the impeller increases. It is worth mentioning that, at the completely dispersed impeller speed, for  $\phi_d$  higher than 0.42 the continuous phase is oil instead of water, as marked by the vertical line in Figure 9. This transition was detected both visually and quantitatively from the ERT measurements.

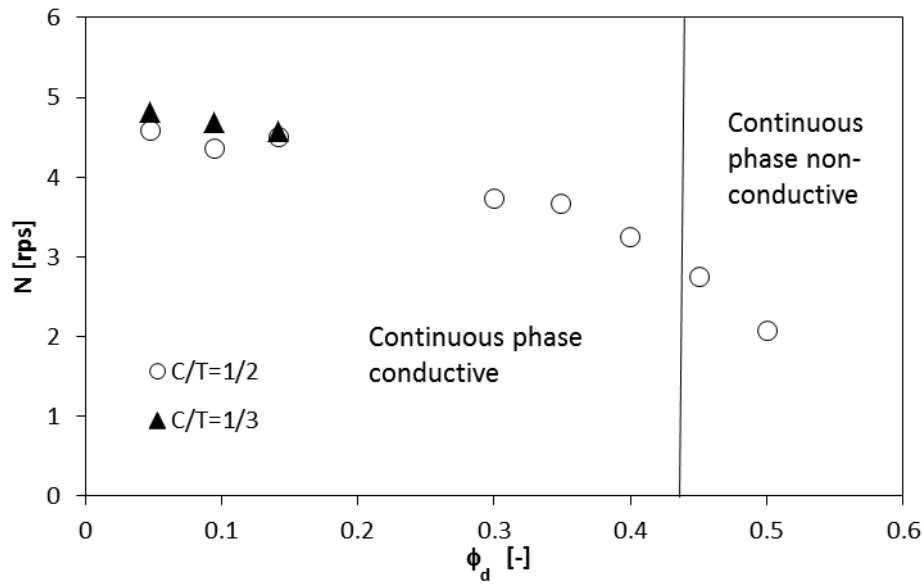


Figure 9. Initial drawdown impeller speed as a function of  $\phi_d$  for two impeller clearances.

The transition between the stratified and the just drawdown condition can be characterised with the impeller Froude number,  $Fr$ , that is the ratio between the inertial and gravitational forces, defined as:

$$Fr = \frac{N^2 D}{g} \quad (6)$$

In addition to the impeller  $Fr$ , that is also adopted to identify the regimes in gas-liquid stirred tanks (Montante and Paglianti, 2015; Warmoeskerken and Smith, 1985), a geometrical parameter, that is the distance between the liquid-liquid interface and the impeller, should also be included in the case of liquid-liquid systems, as clearly indicated from the results shown in Figure 9. From geometrical considerations, this distance can be related to the dispersed phase volume fraction, as:  $z_I - C = T \left| \frac{H_L}{T} (1 - \phi_d) - \frac{C}{T} \right|$ , where  $H_L$  is the height of the mixture inside the tank, that in this work is always equal to  $T$ . Making the distance dimensionless with the impeller diameter, a modified Froude number for identifying the transition,  $Fr'$ , can be computed as:

$$Fr' = Fr \frac{D}{T \left| \frac{H_L}{T} (1 - \phi_d) - \frac{C}{T} \right|} \quad (7)$$

As already proposed by Armenante's group (Tsai, 1988), the lighter phase dispersion can be characterised with the Archimedes number,  $Ar$ , that gives the ratio between the gravitational force on the droplet of size  $d$  and the continuous phase viscous force, as:

$$Ar = \frac{g d^3 \rho_c |\rho_c - \rho_d|}{\mu_c^2} \quad (8)$$

Based on the physical properties and the operating conditions that determine the droplet size, the well-known Weber number theory (Leng and Calabrese, 2016) is adopted for estimating  $d$ , resulting in the following dependency:

$$d = 0.053 D \left( \frac{\sigma}{\rho_c N^2 D^3} \right)^{3/5} \quad (9)$$

If the dispersed liquid is viscous, the internal viscous resistance to the deformation should be considered. In this case, Eq. 9 should be corrected including the viscosity group as suggested by Leng and Calabrese (2016). For the system analysed in present work the correction is below 5%,

therefore it is not used in the following. It is interesting to point out that the accuracy of Eq. 9 has been checked comparing the computed value with the experimental ones obtained with a Spraytec Particle Size Analyzer by Malvern. The test has been carried out at 500 rpm in very dilute conditions, in which coalescence was negligible. The experimental mean Sauter diameter obtained was equal to 47.6 micrometres while the computed value was equal to 72 micrometres. If the correction to take into account the viscosity group is used, a computed value of 76 micrometres is obtained. The equations suggested by Leng and Calabrese (2016) can be used to predict the droplet size with acceptable accuracy within the limits of a factor of 2.

Using  $d$  evaluated by Eq. 9 in Eq. 8, the Archimedes number becomes:

$$Ar = 1.5 \cdot 10^{-4} \frac{g D^3 \left( \frac{\sigma}{\rho_c N^2 D^3} \right)^{9/5} \rho_c |\rho_c - \rho_d|}{\mu_c^2} \quad (10)$$

At the initial drawdown impeller speed, the relationship between the dimensionless numbers defined above is shown in Figure 10.

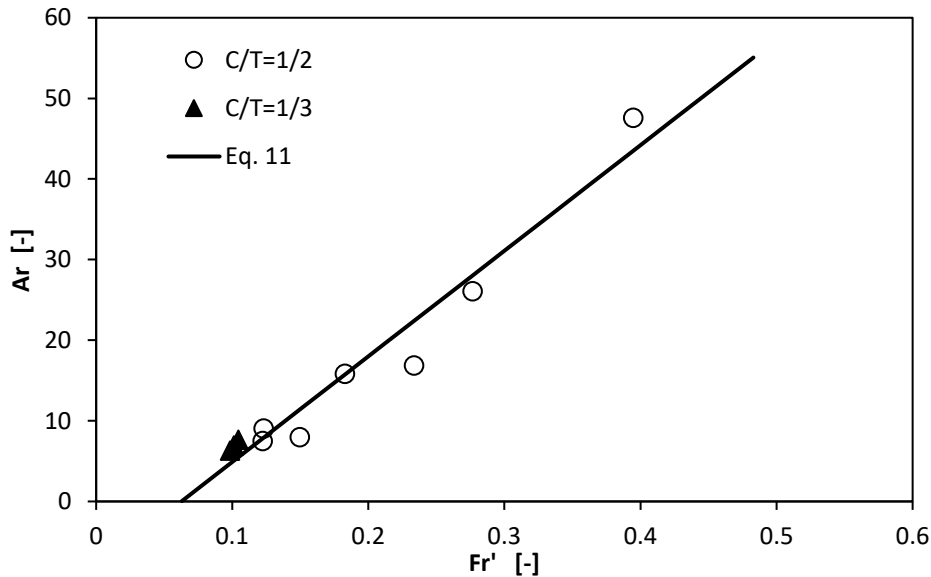


Figure 10. Relationship between  $Ar$  and  $Fr'$  at the initial drawdown impeller speed.



Being the relationship shown in Figure 10 approximately linear, with a simple interpolation of the experimental results the following equation for estimating  $N_{ID}$  can be suggested, at least in the range of conditions investigated in this work:

$$Ar = 131Fr' - 8.21 \quad (11)$$

For comparison with data collected in different systems, only the results reported by Laurenzi et al. (2009), who visually estimated the initial drawdown impeller speed, were found. The investigation was performed using a vessel closed with a lid, that can change the drawdown behaviour. Apart from the geometrical differences, the comparison clearly highlights that the  $N_{ID}$  evaluation performed with the ERT technique is overestimated with respect to the visual observation, since as already observed, ERT is able to catch the transition, measured on a plane distant from  $z_I$ , only if a consistent drawdown occurs.

### 3.2.2 Just dispersed impeller speed, $N_{JD}$

The experimental minimum impeller speed required to eliminate any continuous layer of the dispersed phase is shown in Figure 11 at the different investigated conditions.

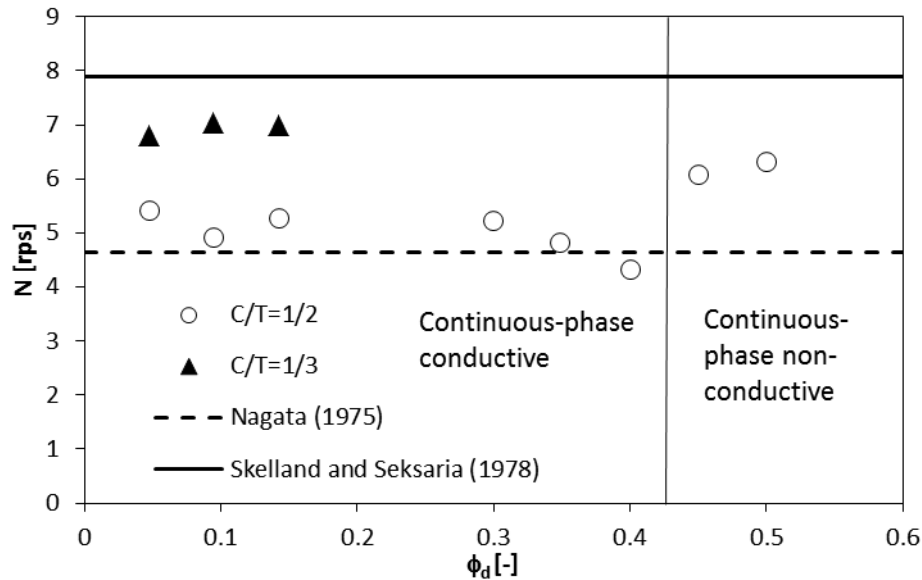


Figure 11. Just dispersed impeller speed as a function of  $\phi_d$  for two impeller clearances.

The vertical line has the same meaning as in Figure 9. While for the case of a conductive continuous phase the transition is identified at low values of  $MI_Z$  on  $z_4$ , for a non-conductive continuous phase, the transition is detected for  $MI_Z$  greater than a critical value on  $z_1$ .

The results in Figure 11 are set between the predictions of the correlations due to Nagata (1975) and Skelland and Seksaria (1978). The experimental data show that the dependency of the just dispersed impeller speed from the dispersed phase volume fraction is weak, while an evident effect of the impeller clearance can be noticed. The same characteristic dimensionless numbers considered in the transition between the stratified and the initial drawdown regimes are considered, apart for the dimensionless geometrical distance, that has a simplified form, since at the just dispersed condition the distance between the impeller and the thin continuous layer is practically located at the liquid free surface. As a result, Eq. 7 becomes:

$$Fr'' = Fr \frac{D}{T \left[ \frac{H_L - C}{T} \right]} \quad (12)$$

The dependency of  $Ar$  and  $Fr''$  at the just dispersed impeller speed is shown in Figure 12 together with literature experimental data of Armenante and Huang (1992) and Laurenzi et al. (2009).

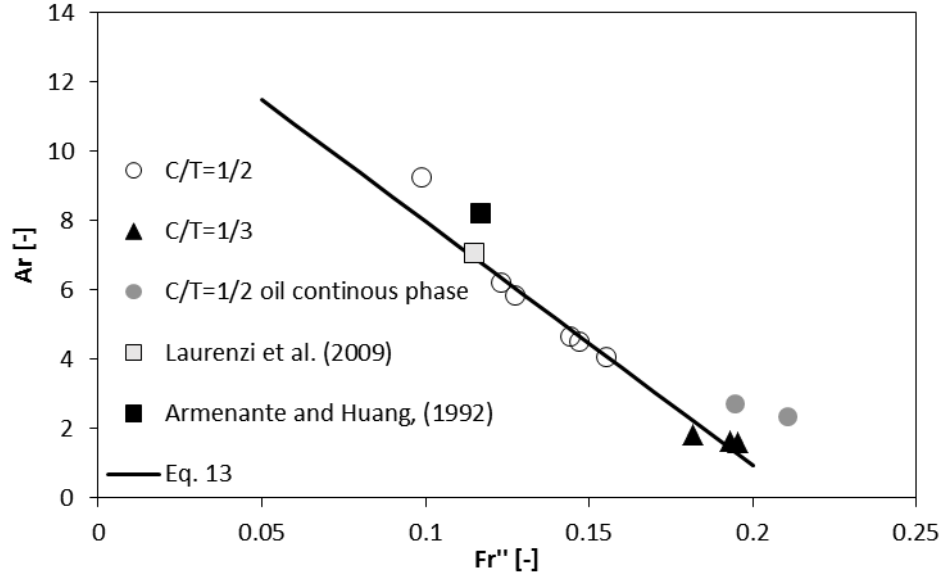


Figure 12. Relationship between  $Ar$  and  $Fr''$  at the just dispersed impeller speed.

For this transition also, the relationship found in Figure 12 is approximately linear. The available experimental data can be interpolated with the following equation, that can be used for estimating the  $N_{JD}$  value:

$$Ar = -70.4Fr'' + 15.0 \quad (13)$$

For estimating the range of application of Eq. (13), the experimental data collected by Armenante's group (Mehta, 2002) using mineral oil, with volume fraction of 0.1, in water are considered. These data are particularly interesting because a detailed analysis on the effect of  $C/T$  and of  $H_L/T$  was performed. Obviously both Equation 11 and 13 can be used only in the range of the physical and geometrical properties tested in the present work. Their use out of this range should be carefully checked. For instance, if the impeller is set close to the free liquid layer the geometrical corrections used in the Froude number can lead to large values of  $Fr''$  and therefore a negative value of  $Ar$ . Future work will be oriented to extend the analysis to these particular geometrical configurations.

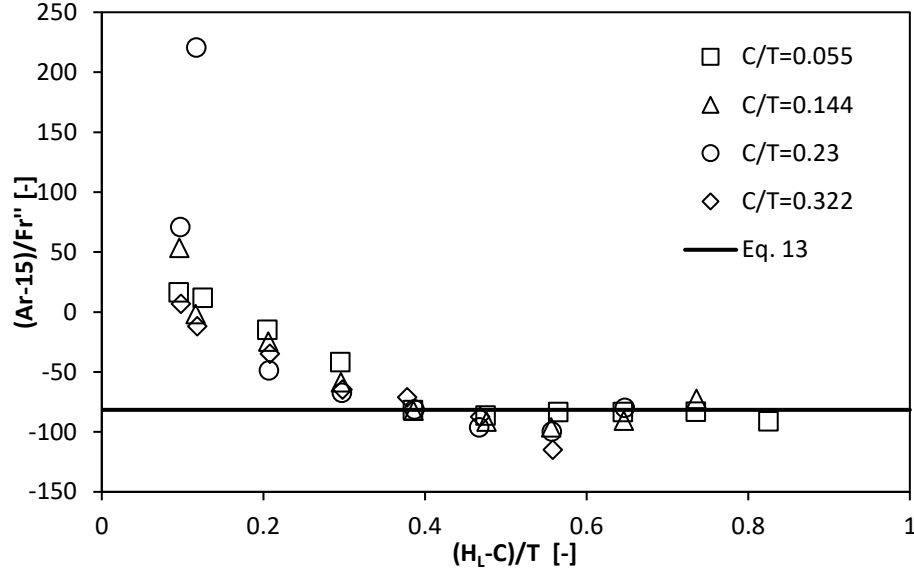


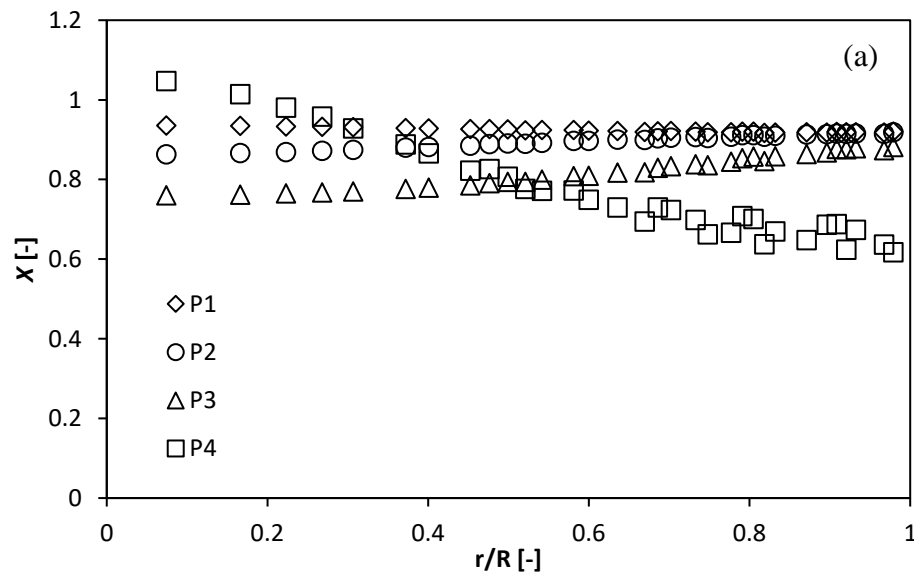
Figure 13. Comparison between Eq.13 and the experimental data of Mehta (2002).

The experimental data reported in Figure 13 show that Eq.13 can be used for predicting the value of  $N_{JD}$  if the ratio  $\frac{H_L-C}{T}$  is greater than 0.3, while for lower values a significant deviation is observed. This result is clearly related to the variation of the fluid dynamics behaviour when the impeller is close to the liquid free surface, as also highlighted from the reduction of the power number measured by Mehta (2002), that cannot be taken in account just by the geometrical dimensionless distance included in the modified Froude number,  $Fr''$ .

Being the completely dispersed condition not detectable visually or by pointwise probes, the advantage of the ERT data are particularly evident in the case of the transition between just drawdown and completely dispersed regimes, that are usually considered as distinct and clearly recognizable (Brown et al., 2004). On the contrary, for the investigated liquid-liquid system at the just dispersed condition, the dispersed liquid was practically homogeneously distributed along the vessel height, as shown by the calculated  $MI_{tot}$  and by the local analysis of the conductivity on the four measurement planes, discussed in the following.

### 3.3 Distribution of the oil droplets throughout the vessel

As already observed in Section 2.3, the fringe effect and the errors in the conductivity field reconstruction when the electrodes are fully immersed in a non-conductive phase, limit the significance of the dimensionless conductivity data obtained using just water as the reference measurement. Consequently, the data can be used to evaluate the volume fraction of the dispersed phase only at impeller speed,  $N$ , equal or higher than that corresponding to the just dispersed condition,  $N_{JD}$ . Instead, at  $N < N_{JD}$  the effect of these issues clearly leads to unreliable dimensionless conductivity profiles, as shown in Figure 14.



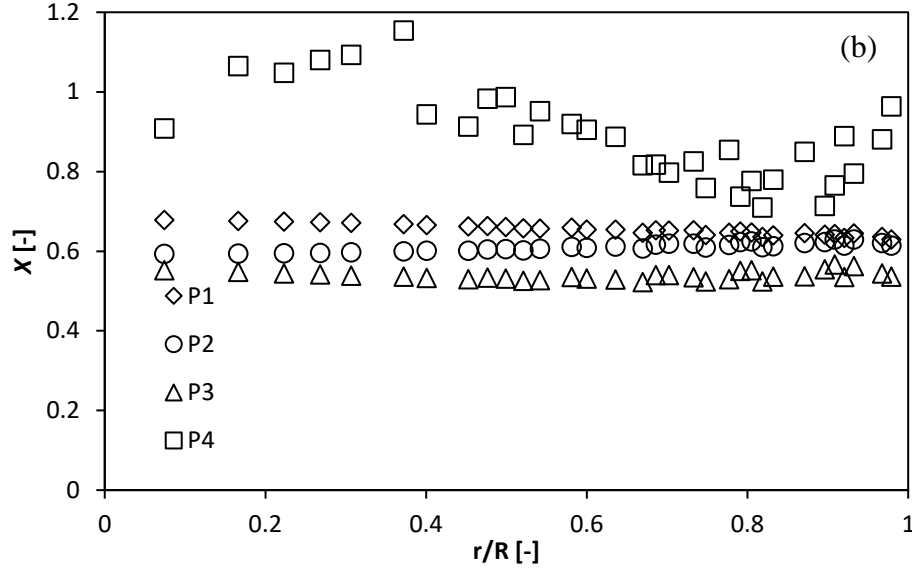


Figure 14. Radial profiles of the dimensionless conductivity. a)  $C/T=1/3$ ,  $\phi_d=14\%$ ,  $N=340$  rpm,

b)  $C/T=1/2$ ,  $\phi_d=35\%$ ,  $N=250$  rpm.

As expected, for low values of  $N$  and high values of  $\phi_d$ , as is the case of the data shown in Figure 14(b), the thickness of the non-conductive layer increases with respect to the case reported in Figure 14(a) and also the measurement error increases. Indeed, local values of the dimensionless conductivity greater than 1 are clearly unphysical, since the maximum value of the dimensionless conductivity should be 1, corresponding to a local value of  $\phi_d$  equal to zero.

Above  $N_{JD}$ , the ERT data are able to properly evaluate the dispersed liquid volume fraction in any section of the vessel, as reported in the Figure 15.

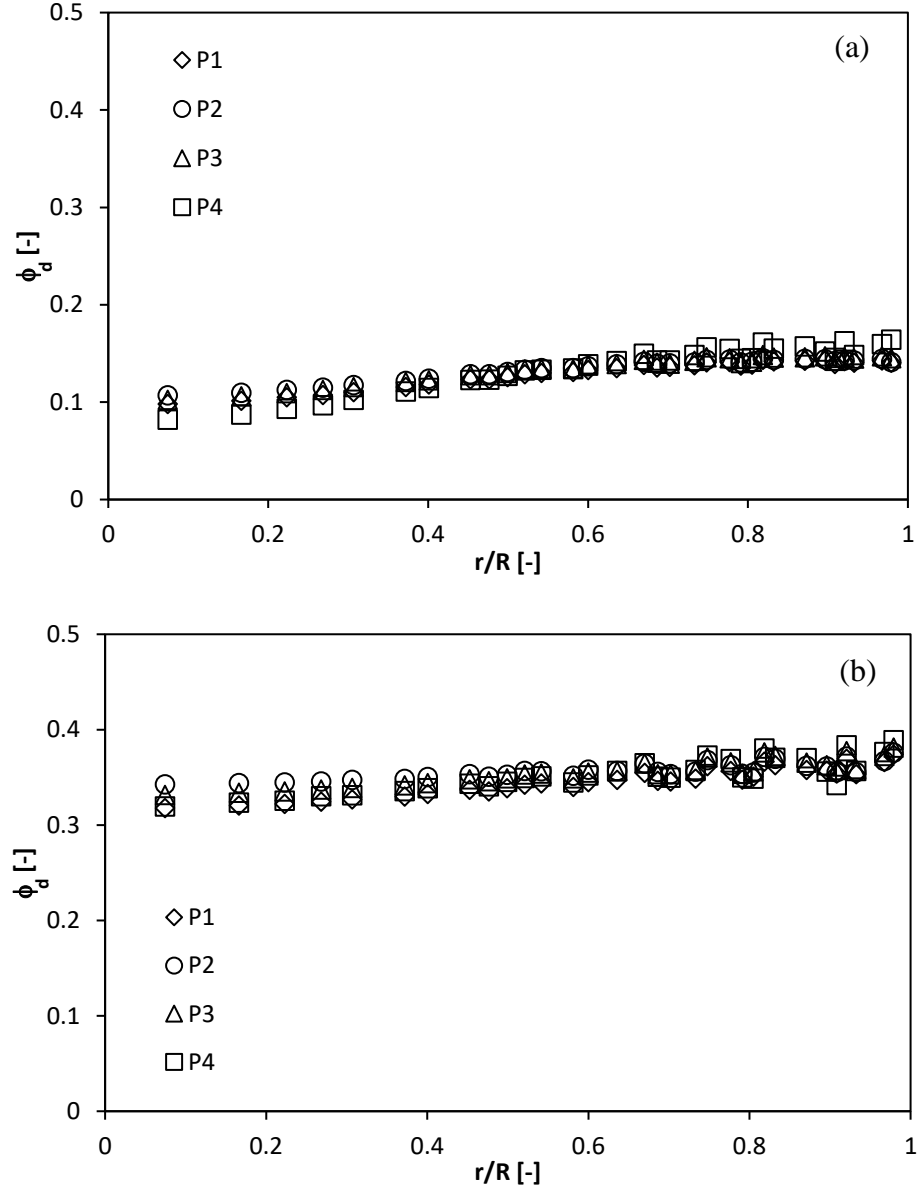


Figure 15. Radial profile of the oil volume fraction. a)  $C/T=1/3$ ,  $\phi_d=14\%$ ,  $N=466$  rpm, b)  $C/T=1/2$ ,  $\phi_d=35\%$ ,  $N=320$  rpm.

The local volume fraction profiles shown in Figure 15 are calculated from the local dimensionless conductivity using the simplified Maxwell equation (Vilar et al., 2008) that for non-conductive spherical particles of equal size reads as:

$$\phi_{d,i} = 2 \frac{(1-X_i)}{(2+X_i)} \quad (14)$$

It is worth noticing that Eq. 14 holds true if the dispersed phase is formed by spherical and uniformly sized dispersed droplets, nonetheless it is commonly used in liquid-liquid (Mirshekari, F., Pakzad, 2019, Bolton et al., 1998) as well as gas-liquid (Forte et al., 2019) and solid-liquid mixtures (Ricard et al., 2005).

As can be observed the liquid droplets are homogeneously distributed along the axial elevation, while an appreciable variation is detected along the radial coordinate. It is worthwhile noticing that the values of the mean volume fraction calculated from the measured values are 14% and 35.8% for the case reported in Figure 15(a) and (b), respectively, that fairly agree with the actual overall oil volume fractions in the vessel that were equal to 14% and 35%.

#### **4. Conclusions**

In this work different liquid-liquid regimes of diesel fuel-water mixture at different volume fractions, impeller speeds and clearances have been investigated.

The measurements helped in the definition of the limits of the ERT technique in liquid-liquid stirred tanks, and the results highlighted that the choice of the reference measurement needed by the non-iterative reconstruction algorithm MSBP affects the results in different ways, depending on the liquid-liquid regime in the vessel.

Four liquid-liquid dispersion regimes were identified, namely the stratified, the initial drawdown, the just dispersed and the completely dispersed regime and different parameters were defined for estimating the regime transitions in different operating conditions.

The study revealed that the initial drawdown impeller speed,  $N_{ID}$ , has a weak dependency on the impeller off-bottom clearance and has a decreasing trend as the volume fraction of dispersed phase increases. The just dispersed impeller speed,  $N_{JD}$ , remains almost constant with the



variation of diesel-fuel volume fraction, but it increases as the impeller off-bottom clearance decreases.

$N_{ID}$  and  $N_{JD}$  dependencies on the Archimedes number and modified Froude numbers were studied finding a linear relationship in the range of operating conditions considered. The results compared well with data from the literature collected in a similar range of operating conditions.

In the conditions considered in this work, the results showed that the completely dispersed regime is achieved once the drawdown is completed. To support this finding, radial profiles of diesel-fuel volume fractions at four different vessel height were analysed and no axial differences were observed at impeller speeds higher than  $N_{JD}$ .

Future investigations will be addressed to apply the methodology devised in this work to different liquid-liquid systems, for covering a wide range of industrially relevant physical properties of the two immiscible phases and assessing their effect on the liquid-liquid mixing feature discussed in this work.

## **Acknowledgment**

A. Paglianti acknowledges the support of the Italian Government through the Grant "Excellent Departments" 2018-2022. The collaboration of Teresa Megna, Eugenia Tugnoli and Manuel Boschi in carrying out part of the experimental program is gratefully acknowledged.

## **Nomenclature**

$Ar$	Archimedes number, dimensionless
$C$	impeller off-bottom clearance, m
$d$	droplet size, m

D	impeller diameter, m
Fr	Froude number, dimensionless
g	gravity acceleration, m s <sup>-2</sup>
H	vessel height, m
H <sub>L</sub>	liquid height, m
MI <sub>tot</sub>	total mixing index (Eq. 5), dimensionless
MI <sub>z</sub>	mixing index on selected plane (Eq.4), dimensionless
n	number of local measurements on a plane, dimensionless
N	impeller speed, s <sup>-1</sup>
N <sub>ID</sub>	initial drawdown impeller speed, s <sup>-1</sup>
N <sub>JD</sub>	just dispersed impeller speed, s <sup>-1</sup>
p	total number of local measurements on the four planes, dimensionless
r	radial coordinate, m
R	radius of the vessel, m
T	vessel diameter, m
z	axial coordinate, m
X <sub>i</sub>	local dimensionless conductivity
$\bar{X}$	mean dimensionless conductivity

### ***Greek letters***

$\phi_d$	diesel fuel volume fraction, dimensionless
$\gamma_i$	local conductivity, S/m
$\gamma_i^{ref}$	local conductivity of the reference measurement, S/m

$\mu_c$	continuous phase dynamic viscosity, kg/m/s
$\mu_d$	dispersed phase dynamic viscosity, kg/m/s
$\rho_c$	continuous phase density, kg/m <sup>3</sup>
$\rho_d$	dispersed phase density, kg/m <sup>3</sup>
$\sigma$	interfacial tension, N/m
$\sigma_c$	continuous phase surface tension, N/m
$\sigma_d$	dispersed phase surface tension, N/m

## References

- Afshar Ghotli, R., Raman, A.A.A., Ibrahim, S., Baroutian, S., 2013. Liquid-liquid mixing in stirred vessels: a review. *Chem. Eng. Commun.* 200, 595–627. <https://doi.org/10.1080/00986445.2012.717313>
- Alopaeus, V., Koskinen, J., I. Keskinen, K., Majander, J., 2002. Simulation of the population balances for liquid–liquid systems in a nonideal stirred tank. Part 2—parameter fitting and the use of the multiblock model for dense dispersions. *Chem. Eng. Sci.* 57, 1815–1825. [https://doi.org/10.1016/S0009-2509\(02\)00067-2](https://doi.org/10.1016/S0009-2509(02)00067-2)
- Armenante, P.M., Huang, Y.T., 1992. Experimental determination of the minimum agitation speed for complete liquid-liquid dispersion in mechanically agitated vessels. *Ind. Eng. Chem. Res.* 31, 1398–1406. <https://doi.org/10.1021/ie00005a022>
- Bałdyga, J., Bourne, J.R., Pacek, A.W., Amanullah, A., Nienow, A.W., 2001. Effects of agitation and scale-up on drop size in turbulent dispersions: allowance for intermittency. *Chem. Eng. Sci.* 56, 3377–3385. [https://doi.org/10.1016/S0009-2509\(01\)00027-6](https://doi.org/10.1016/S0009-2509(01)00027-6)
- Bolton, G.T., Korchinsky, W.J., Waterfall, R.C., 1998. Calibration of capacitance tomography systems for liquid-liquid dispersions. *Meas. Sci. Technol.* 9, pp. 1797-1800
- Bowler, A.L., Bakalis, S., Watson, N. J., 2020. A review of in-line and on-line measurement techniques to monitor industrial mixing processes. *Chem. Eng. Res. Des.* 153, 463–495. <https://doi.org/10.1016/j.cherd.2019.10.045>
- Brown, D.A., Jones, P., Middleton, J.C., Papadopoulos, G., Arik, E.B., 2004. Experimental methods, in: Paul, E.L., Atiemo-Obeng, V.A., Kresta, S.M. (Eds.), *Handbook of Industrial Mixing: Science and Practice*. John Wiley & Sons Inc., Hoboken, New Jersey, pp. 145--256.
- Calabrese, R. V., Wang, C.Y., Bryner, N.P., 1986. Drop breakup in turbulent stirred-tank

contactors. Part III: Correlations for mean size and drop size distribution. *AIChE J.* 32, 677–681.

<https://doi.org/10.1002/aic.690320418>

Carletti, C., Montante, G., Westerlund, T., Paglianti, A., 2014. Analysis of solid concentration distribution in dense solid–liquid stirred tanks by electrical resistance tomography. *Chem. Eng. Sci.* 119, 53–64. <https://doi.org/10.1016/j.ces.2014.07.049>

Daglas, D., Stamatoudis, M., 2000. Effect of impeller vertical position on drop sizes in agitated dispersions. *Chem. Eng. Technol.* 23, pp. 437–440.

De Bona, J., Buffo, A., Vanni, M., Marchisio, D.L., 2016. Limitations of simple mass transfer models in polydisperse liquid-liquid dispersions. *Chem. Eng. J.* 296, pp. 112–121.

Derksen, J.J., Van Den Akker, H.E.A., 2007. Multi-Scale Simulations of Stirred Liquid–Liquid Dispersions. *Chem. Eng. Res. Des.* 85, 697–702. <https://doi.org/10.1205/cherd06161>

Du, X., Duan, X., Yang, C. 2019. Visual Study on the Interphase Mass Transfer of Immiscible Liquid-Liquid System in a Stirred Tank. *Ind. Eng. Chem. Res.* 58, 21785–21796. <https://doi.org/10.1021/acs.iecr.9b05060>

Duan, S., Meng, X., Zhang, R., Jian H-L, Xu J., Du W., Xu, C., Liu, Z., 2019. Experimental and Computational Investigation of Mixing and Separation Performance in a Liquid-Liquid Cyclone Reactor. *Ind. Eng. Chem. Res.* 58, pp. 23317–23329.

Elghobashi, S. 2019. Direct numerical simulation of turbulent flows laden with droplets or bubbles. *Annual Review of Fluid Mechanics*, 51, 217–244. <https://doi.org/10.1146/annurev-fluid-010518-040401>.

Forte, G., Alberini, F., Simmons, M.J.H., Stitt, E.H., 2019. Measuring gas hold-up in gas–liquid/gas–solid–liquid stirred tanks with an electrical resistance tomography linear probe. *AIChE J.*, 65, art. no. e16586. <https://doi.org/10.1002/aic.16586>

- Harrison, S.T.L., Kotsiopoulos, A., Stevenson, R., Cilliers, J.J., 2020. Mixing indices allow scale-up of stirred tank slurry reactor conditions for equivalent homogeneity. *Chem. Eng. Res. Des.*, 153, 865-874. <https://doi.org/10.1016/j.cherd.2019.10.049>.
- Hemrajani, R. R., Tatterson, G. B., 2004. Mechanically stirred vessels., in: Paul, E.M, Atiemo-Obeng, V.A., Kresta, S.M. (Eds.), *Handbook of Industrial Mixing*. Wiley & Sons, Inc., Hoboken, New Jersey, pp. 345-389.
- Hohl, L., Röder, V., Kraume, M., 2019. Dispersion and Phase Separation of Water-Oil-Amphiphile Systems in Stirred Tanks. *Chem. Eng. Technol.* 42, pp. 1574-1586.
- Kamil, M., Bushra, A., Ahmad, A., 2001. Minimum agitation speed for liquid–liquid–gas dispersion in mechanically agitated vessels. *Chem. Eng. Process. Process Intensif.* 40, 49–57. [https://doi.org/10.1016/S0255-2701\(00\)00110-0](https://doi.org/10.1016/S0255-2701(00)00110-0)
- Kamp, J., Kraume, M., 2016. From single drop coalescence to droplet swarms – Scale-up considering the influence of collision velocity and drop size on coalescence probability. *Chem. Eng. Sci.* 156, 162–177. <https://doi.org/10.1016/j.ces.2016.08.028>
- Kazemzadeh, A., Ein-Mozaffari, F., Lohi, A., Pakzad, L., 2016. A new perspective in the evaluation of the mixing of biopolymer solutions with different coaxial mixers comprising of two dispersing impellers and a wall scraping anchor. *Chem. Eng. Res. Des.*, 114, 202-219. <https://doi.org/10.1016/j.cherd.2016.08.017>.
- Komrakova, A.E., Eskin, D., Derksen, J.J., 2015. Numerical study of turbulent liquid-liquid dispersions. *AIChE J.* 61, 2618–2633. <https://doi.org/10.1002/aic.14821>
- Laurenzi, F., Coroneo, M., Montante, G., Paglianti, A., Magelli, F., 2009. Experimental and computational analysis of immiscible liquid–liquid dispersions in stirred vessels. *Chem. Eng. Res. Des.* 87, 507–514. <https://doi.org/10.1016/j.cherd.2008.12.007>

Leng, D.E., Calabrese, R. V., 2016. Immiscible Liquid-Liquid Systems, in: Kresta, S.M., Etchells, A.W.I., Dickey, D.S., Atiemo-Obeng, V.A. (Eds.), *Advances in Industrial Mixing: A Companion to the Handbook of Industrial Mixing*. Wiley & Sons, Inc., Hoboken, New Jersey, pp. 457–463.

Li, D., Gao, Z., Buffo, A., Podgorska, W., Marchisio, D.L., 2017. Droplet breakage and coalescence in liquid-liquid dispersions: Comparison of different kernels with EQMOM and QMOM. *AIChE J.* 63, 2293–2311. <https://doi.org/10.1002/aic.15557>

Liang, W., Wang, D., Cai, Z., Li, Z., Huang, X., Gao, Z., Derksen, J.J., Komrakova, A.E., 2019. Deformation and breakup of single drop in laminar and transitional jet flows. *Chem. Eng. J.* <https://doi.org/10.1016/j.cej.2019.05.173>

Lioumbas, J.S., Chatzidafni, A., Karapantsios, T.D., 2014. Spatial considerations on electrical resistance tomography measurements. *Meas. Sci. Technol.* 25, 055303. <https://doi.org/10.1088/0957-0233/25/5/055303>

Maaß, S., Gäbler, A., Zaccone, A., Paschedag, A.R., Kraume, M., 2007. Experimental Investigations and Modelling of Breakage Phenomena in Stirred Liquid/Liquid Systems. *Chem. Eng. Res. Des.* 85, 703–709. <https://doi.org/10.1205/cherd06187>

Maaß, S., Metz, F., Rehm, T., Kraume, M., 2010. Prediction of drop sizes for liquid–liquid systems in stirred slim reactors—Part I: Single stage impellers. *Chem. Eng. J.* 162, 792–801. <https://doi.org/10.1016/j.cej.2010.06.007>

Maaß, S., Paul, N., Kraume, M., 2012. Influence of the dispersed phase fraction on experimental and predicted drop size distributions in breakage dominated stirred systems. *Chem. Eng. Sci.* 76, 140–153. <https://doi.org/10.1016/j.ces.2012.03.050>

Maaß, S., Wollny, S., Sperling, R., Kraume, M., 2009. Numerical and experimental analysis of

particle strain and breakage in turbulent dispersions. *Chem. Eng. Res. Des.* 87, 565–572.

<https://doi.org/10.1016/j.cherd.2009.01.002>

Mehta, S., 2002. Liquid-liquid mixing in stirred tanks with varying liquid depths. New Jersey Institute of Technology.

Mirshekari, F., Pakzad, L., 2019. Mixing of Oil in Water Through Electrical Resistance Tomography and Response Surface Methodology. *Chem. Eng. Technol.*, 42, 1101-1115.

<https://doi.org/10.1002/ceat.201800563>

Mirshekari, F., Pakzad, L., Fatehi, P. 2019 An investigation on the stability of the hazelnut oil-water emulsion *J. Dispersion Sci. Technol.* published on-line

<https://doi.org/10.1080/01932691.2019.1614459>

Montante, G., Paglianti, A., 2015. Gas hold-up distribution and mixing time in gas–liquid stirred tanks. *Chem. Eng. J.* 279, 648–658. <https://doi.org/10.1016/j.cej.2015.05.058>

Nagata, S., 1975. *Mixing: Principles and applications*. John Wiley & Sons Inc., New York.

Naeeni, S.K., Pakzad, L., 2019. Experimental and numerical investigation on mixing of dilute oil in water dispersions in a stirred tank. *Chem. Eng. Res. Des.* 147, 493–509.

<https://doi.org/10.1016/j.cherd.2019.05.024>

Podgórska, W., 2005. Scale-up effects in coalescing dispersions—comparison of liquid–liquid systems differing in interface mobility. *Chem. Eng. Sci.* 60, 2115–2125.

<https://doi.org/10.1016/j.ces.2004.10.035>

Podgórska, W., Bałdyga, J., 2001. Scale-up effects on the drop size distribution of liquid–liquid dispersions in agitated vessels. *Chem. Eng. Sci.* 56, 741–746. [https://doi.org/10.1016/S0009-2509\(00\)00284-0](https://doi.org/10.1016/S0009-2509(00)00284-0)

Ricard, F., Brechtelsbauer, C., Xu, X.Y., Lawrence, C.J., 2005. Monitoring of Multiphase



Pharmaceutical Processes Using Electrical Resistance Tomography. *Chem. Eng. Res. Des.* 83, 794–805. <https://doi.org/10.1205/cherd.04324>

Skelland, A.H.P., Ramsay, G.G., 1987. Minimum agitator speeds for complete liquid-liquid dispersion. *Ind. Eng. Chem. Res.* 26, 77–81. <https://doi.org/10.1021/ie00061a014>

Skelland, A.H.P., Seksaria, R., 1978. Minimum Impeller Speeds for Liquid-Liquid Dispersion in Baffled Vessels. *Ind. Eng. Chem. Process Des. Dev.* 17, 56–61. <https://doi.org/10.1021/i260065a010>

Solsvik, J., Jakobsen, H.A., 2015. Single drop breakup experiments in stirred liquid–liquid tank. *Chem. Eng. Sci.* 131, 219–234. <https://doi.org/10.1016/j.ces.2015.03.059>

Stanley, S.J., 2006. Tomographic imaging during reactive precipitation in a stirred vessel: Mixing with chemical reaction. *Chem. Eng. Sci.* 61, 7850–7863. <https://doi.org/10.1016/j.ces.2006.09.029>

Sun, J., Yang, W., 2013. Fringe effect of electrical capacitance and resistance tomography sensors. *Meas. Sci. Technol.* 24, 074002. <https://doi.org/10.1088/0957-0233/24/7/074002>

Tsai, D.-H., 1988. Agitation requirements for complete dispersion of emulsions. New Jersey Institute of Technology, Theses 1408. <https://digitalcommons.njit.edu/theses/1408>.

Tsouris, C., Lizama, H.M., Spurrier, M.A., Takeuchi, T.L., Scott, T.C., 1996. Hydrodynamics of bioreactor systems for liquid-liquid contacting. *Appl. Biochem. Biotechnol.* 57-58, pp. 581-592.

Vilar, G., Williams, R.A., Wang, M., Tweedie, R.J., 2008. On line analysis of structure of dispersions in an oscillatory baffled reactor using electrical impedance tomography. *Chem. Eng. J.* 141, 58–66. <https://doi.org/10.1016/j.cej.2007.10.018>

Vonka, M., Soos, M., 2015. Characterization of liquid-liquid dispersions with variable viscosity by coupled computational fluid dynamics and population balances. *AIChE J.* 61, 2403–2414.

<https://doi.org/10.1002/aic.14831>

Wang, M., Mann, R., Dickin, F.J., Dyakowski, T., 1996. Large-scale Electrical Tomography Sensing System to Study Mixing Phenomena, in: Proceedings IWISP '96. Elsevier, pp. 647–650.

<https://doi.org/10.1016/B978-044482587-2/50142-7>

Warmoeskerken, M.M.C.G., Smith, J.M., 1985. Flooding of disc turbines in gas-liquid dispersions: A new description of the phenomenon. Chem. Eng. Sci. 40, 2063–2071.

[https://doi.org/10.1016/0009-2509\(85\)87023-8](https://doi.org/10.1016/0009-2509(85)87023-8)

Zhao, Y., Li, X., Cheng, J., Yang, C., Mao, Z.-S., 2011. Experimental study on liquid-liquid macromixing in a stirred tank. Ind. Eng. Chem. Res. 50, pp. 5952-5958.

Zhou, G., Kresta, S.M., 1998. Correlation of mean drop size and minimum drop size with the turbulence energy dissipation and the flow in an agitated tank. Chem. Eng. Sci. 53, 2063–2079.

[https://doi.org/10.1016/S0009-2509\(97\)00438-7](https://doi.org/10.1016/S0009-2509(97)00438-7)